

GMRT OBSERVATIONS OF IC 711 – THE LONGEST HEAD-TAIL RADIO GALAXY KNOWN

SHWETA SRIVASTAVA¹ AND ASHOK K. SINGAL²

ASTRONOMY & ASTROPHYSICS DIVISION, PHYSICAL RESEARCH LABORATORY,
 NAVRANGPURA, AHMEDABAD - 380 009, INDIA

¹shweta@prl.res.in, ²asingal@prl.res.in

(Received)

Draft version October 26, 2016

ABSTRACT

We present low-frequency, Giant Metrewave Radio Telescope (GMRT) observations at 240, 610 and 1300 MHz of IC 711, a narrow angle tail (NAT) radio galaxy. The galaxy lies in Abell cluster 1314 (redshift ~ 0.034) and has a long radio tail of total angular extent ~ 17 arcmin, corresponding to a projected linear size of ~ 700 kpc. This makes it the longest head-tail radio galaxy known. The objectives of the GMRT observations were to investigate the diffuse-emission of the long tail structure at low frequencies. The radio structure, especially initial ~ 10 arcmin of tail being a long straight feature, does not seem to be consistent with a simple circular motion around the cluster centre, as previously suggested in the literature. Two sharp bends after the straight section of the tail cast doubt on the prevailing idea in the literature that the long narrow tails represent trails left behind by the fast moving parent optical galaxy with respect to the cluster medium, as the optical galaxy could not have undergone such sharp bends in its path, under any conceivable gravitational influence of some individual galaxy or of the overall cluster gravitational potential. In fact the tail does not seem to have been influenced by the gravitational field of any of the cluster-member galaxy. The radio tail shows a break in the spectrum. We derive an expression for the minimum energy in the case of a spectral break, in order to do the minimum energy calculation in diffuse tail regions of IC 711.

Subject headings: galaxies: active — galaxies: jets — radiation mechanisms: non-thermal — radio continuum: galaxies

1. INTRODUCTION

Radio galaxies found in clusters of galaxies often show very striking structural features not seen among those outside clusters. These include narrow angle tails (NATs), wide angle tails (WATs), and some other peculiar morphologies (see e.g., Miley 1980; O’Dea and Owen 1985; Owen and Ledlow 1997), which hopefully shed light on both the radio galaxy and its interaction with the cluster medium.

The interaction between the radio sources in the clusters and the cluster environment is not well understood (Feretti & Giovannini 2008). Radio galaxies in the same or similar types of clusters are often found to be very different in their radio morphologies. One possible explanation for the difference in radio structures is the difference in the relative speed of the parent galaxy with respect to the surrounding intra-cluster medium (ICM) or differences within the ICM at the location of these radio galaxies. As the radio jets propagate through ICM, variations in the ICM density and velocity may account for the complex radio morphologies that are observed. Of course the energy budget of the radio galaxies in question must also be playing a crucial role while interacting with the ICM. A difference in the radio ages of the galaxies may also influence their appearance.

In this paper, we present low-frequency, GMRT observations at 240, 610 and 1300 MHz of IC 711, a long head-tail radio galaxy. The galaxy lies in Abell cluster 1314 (redshift $z \sim 0.034$) which hosts another radio galaxy IC 708 in the peculiar shape of a highly bent WAT. The radio structures of the radio galaxies IC 711 and IC 708 are very dissimilar. The radio galaxy IC 711 has a nar-

row long tail of total angular extent ~ 17 arcmin. On the other hand IC 708 has a rather ‘squat’ radio morphology, with a wide-angle tail structure with a maximum extension of about 2 arcmin. These two objects have been studied with the Westerbork telescope (Vallée & Wilson 1976; Wilson & Vallée 1977; Jägers 1987; Vallée & Strom 1988) and the Very Large Array (O’Dea and Owen 1985; Owen & Ledlow 1997). Our objectives for GMRT observations were to investigate the diffuse-emission of the long tail structure of IC 711 at low frequencies and to explore what further constraints can be put on the prevalent ideas in literature about the formation of the head-tail morphologies.

2. OBSERVATIONS

The GMRT observations were made at 240, 610 and 1300 MHz on 2015 July. The GMRT consists of thirty 45-m antennas in an approximate ‘Y’ shape similar to the Very Large Array but with each antenna in a fixed position. Twelve antennas are randomly placed within a central $1 \text{ km} \times 1 \text{ km}$ square (the ‘Central Square’) and the remainder form the irregularly shaped Y (6 on each arm) over a total extent of about 25 km. Further details about the array can be found at the GMRT website at <http://www.gmrt.ncra.tifr.res.in>. The observations were made in the standard fashion, with each source observation interspersed with observations of the phase calibrator. The source was observed in dual (610/240 MHz) frequency mode for 8 hours, although a small percentage of data had to be edited out due to ionospheric disturbances. The primary flux 3C286 whose flux density were estimated to be 52.6 and 67.1 at 240 MHz, 29.1 and 20.6 density calibrator was 3C286 whose flux den-

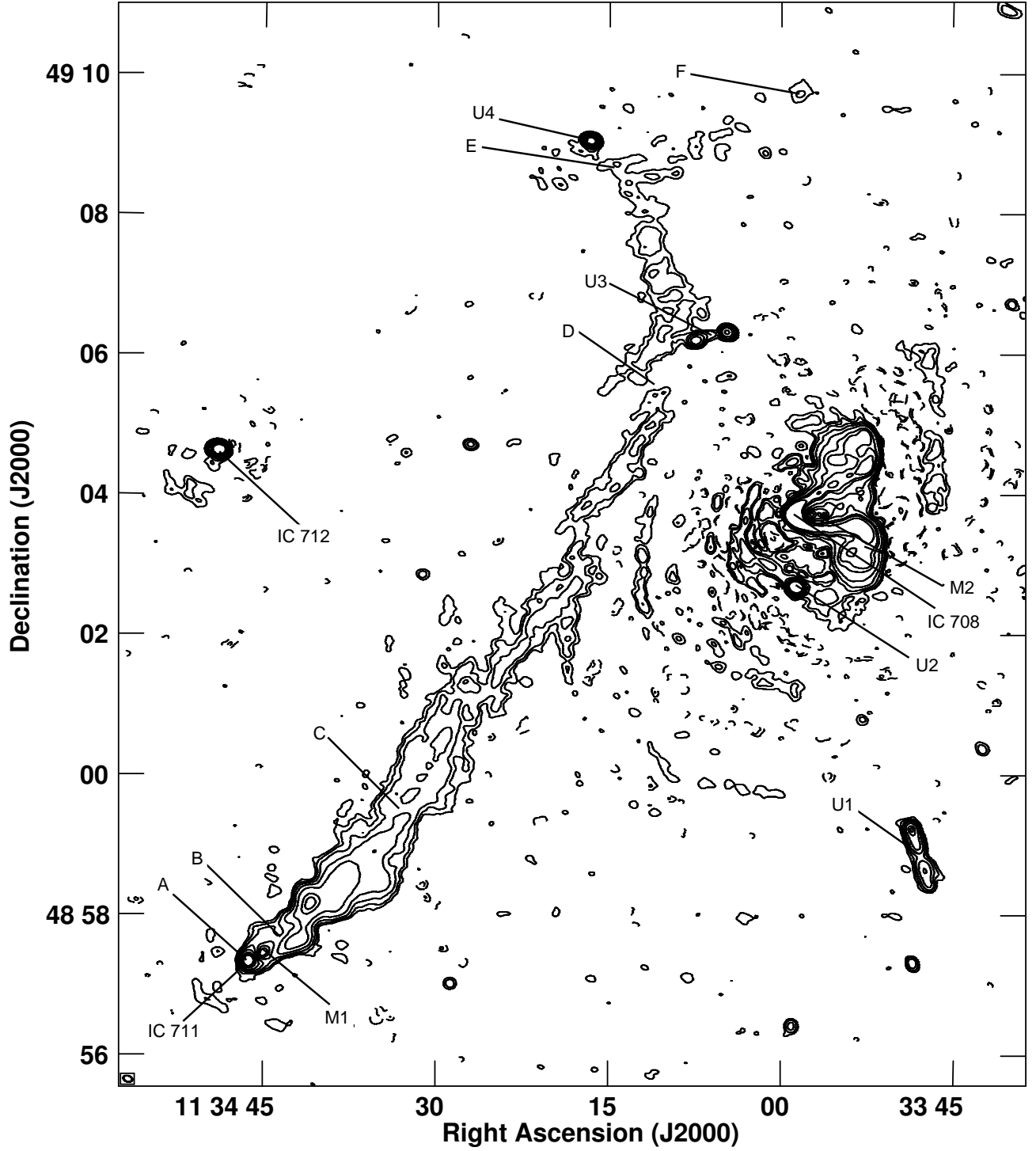


Figure 1. 610 MHz contour image of IC 711. The contour levels are $0.046 \times (-4, 4, 8, 16, 32, 64, 128, 256)$ mJy beam $^{-1}$. A is the compact head that coincides with the optical galaxy IC 711, while B, C, D, E, F indicate various sections of the tail. IC 708 and IC 712 are other radio galaxies in the cluster. U1, U2, U3, U4 are optically unidentified radio sources in the field. M1, M2 are actually minima (see text).

Table 1. The observational parameters of GMRT

Frequency MHz	Beam size			rms
	"	"	°	mJy/b
(1)	(2)	(3)	(4)	(5)
240	12.3	8.1	82	1.15
610	7.8	5.2	71	0.04
1300	2.7	2.2	36	0.02

Column 1: frequency of observations in units of MHz, columns 2-4: the major and minor axes of the restoring beam in arcsec and its PA in degrees; column 5: the rms noise in units of mJy/beam.

sity was estimated to be 67.1 Jy at 240 MHz, 20.6 Jy at 610 MHz, and 15.7 Jy at 1300 MHz. The phase calibrator was 3C241 whose flux density was estimated to be 10.65 ± 0.62 Jy at 240 MHz, 4.53 ± 0.02 Jy at 610 MHz and 2.03 ± 0.04 Jy at 1300 MHz. The data analyses were done using the Astronomical Image Processing Software (AIPS) of the National Radio Astronomy Observatory. The total flux densities of different sources or tail components of IC711 were measured using the AIPS task TVSTAT, which allows us to pick an area of any shape. Error on the flux density of a component was obtained by multiplying the average noise rms with \sqrt{N} where N is the total area of the component measured in units of synthesized beams.

The observational parameters of the GMRT beams for different frequencies are listed in Table 1.

3. RESULTS AND DISCUSSION

The GMRT images of IC 711 at 610 MHz is presented in Fig. 1. The 610-MHz image with an angular resolution of $7.''8 \times 5.''2$ along a position angle of 71° , shows the radio galaxy IC 711 having a long tail of total angular extent ~ 17 arcmin. This high resolution map shows that the radio tail along its stretch is initially straight for two-thirds (~ 10 arcmin) of its length, then there is a sharp (almost a 90°) bend after ~ 4 arcmin, and then further along there is an other similar sharp bend pointing away from the cluster center and the diffuse source tail continues for another ~ 3 arcmin. There are a number of prominent radio sources (U1,U2,U3,U4) which remain unidentified optically and most likely are unrelated to the Abell cluster 1314 and are merely background radio sources and in at least two of them (U1 and U3) the double radio structure is clearly seen in 610 MHz map (Fig. 1) and also in the 1300 MHz map (Fig. 3).

Figure 2 shows a higher resolution contour map of the head and the front part of the tail at 1300 MHz, superimposed on the grey scale map of the same region at 610 MHz. The unresolved head and twin jets emanating on both sides are clearly seen as modelled first by Begelman et al. (1979). We may like to point out that at 610 MHz the gap between the twin jets which is clearly seen in Fig. 2 is not seen clearly in Fig. 1, where it looks like a brighter region (M1), which in reality is a local minima. This is because of the inability of the AIPS contour maps to properly display a less intense region surrounded on all sides by more brighter regions and which can be seen properly only on a grey scale/color map.

Figure 3 shows the low resolution 1300 MHz contour map, superimposed on the 50 cm grey scale map. The 20 cm (1300 MHz) contour map was convolved with a broader beam so as to make the diffuse tail regions visible which were not so in the higher resolution map. Even

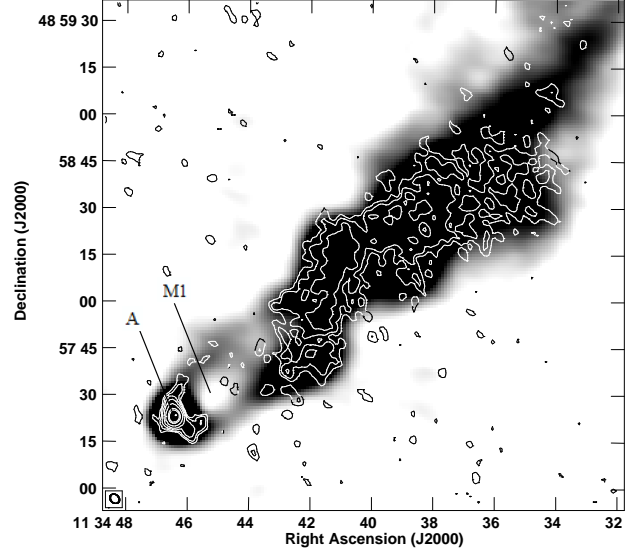


Figure 2. 1300 MHz high resolution map of the head and the front part of the tail superimposed on the 610 MHz grey scale map of the same region. The contour levels are $0.065 \times (-3, 3, 6, 12, 24, 48, 96)$ mJy beam $^{-1}$.

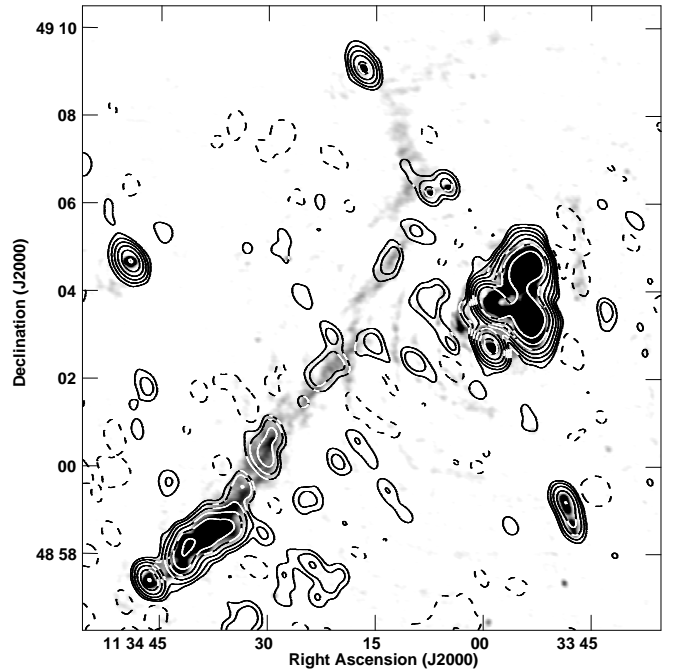


Figure 3. A low resolution ($30'' \times 20''$ along PA = 32°) 1300 MHz contour image of IC 711 superimposed on the grey scale map at 610 MHz. The 1300 MHz contour levels are $0.23 \times (-3, 3, 6, 12, 24, 48, 96, 192)$ mJy beam $^{-1}$.

though the tail emission is quite weak at 1300 MHz, still it is clear that it largely follows the tail emission at 610 MHz, as seen in the grey scale map.

Figure 4 shows the 240 MHz map of the radio galaxy IC 711 overlaid over optical field, where positions of prominent optical galaxies are marked. None of the galaxy seems to have any direct gravitational influence on the long radio tail which shows essentially the same features as seen in the 610 MHz map in Fig. 1.

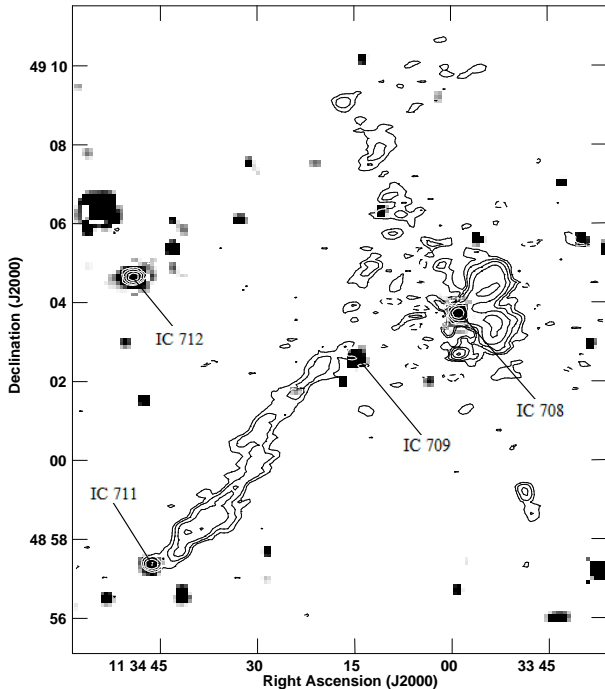


Figure 4. The 240 MHz map overlaid over Optical field. Prominent cluster galaxies in the field are marked. The contour levels for the 240 MHz map are $1.1 \times (-3, 3, 6, 12, 32, 24, 48)$ mJy beam $^{-1}$.

IC708 (Fig. 5) has a wide-angle tail radio structure. The twin jets show multiple knots and end up in “hot-spots”, flanked by two diffuse radio lobes, marked N (north) and S (south). This galaxy has been discussed in detail by Vallée et al. (1979, 1981). Here we want to point out that in the 610 MHz contour map (Fig. 1) the apparently brightest feature M2 (like M1) is actually a minima and represents the gap between the twin jets which is clearly seen in Fig. 5. Further, the overlap between the 1300 MHz emission, represented by contour map in Fig. 5, and the 610 MHz emission, shown as a grey scale map, is excellent, both in the twin jets as well as in the extended lobes.

The overall angular size of IC 711 extending to 17 arcmin which translates to a physical size of about 700 kpc size ($H_0 = 70$ km s $^{-1}$ Mpc) at the cluster redshift of 0.034. This makes it perhaps the longest head-tail radio galaxy known. With giant radio galaxies defined as having a physical size ~ 700 kpc or greater for $H_0 = 70$ km s $^{-1}$ Mpc $^{-1}$ (which translates to > 1 Mpc for $H_0 = 50$ km s $^{-1}$ Mpc $^{-1}$, conventionally defined as a giant radio galaxy; Saripalli et al. 2005), IC 711 is the only example of a non-FRII radio galaxy being the size of a giant radio galaxy. Either of the bends in the tail of IC 711 seems to occur very close to another radio source, though it is not sure whether the bend is really related to that radio object. We are not even sure whether the radio sources close to the bends are the cluster-members, since no optical galaxy is found at either of them. Therefore either or both of these two radio sources could be background (or even foreground) objects, though the bending of the tail at so close to each of them in sky position is a very striking feature. There seems to be no direct gravitational influence of any of the prominent cluster members

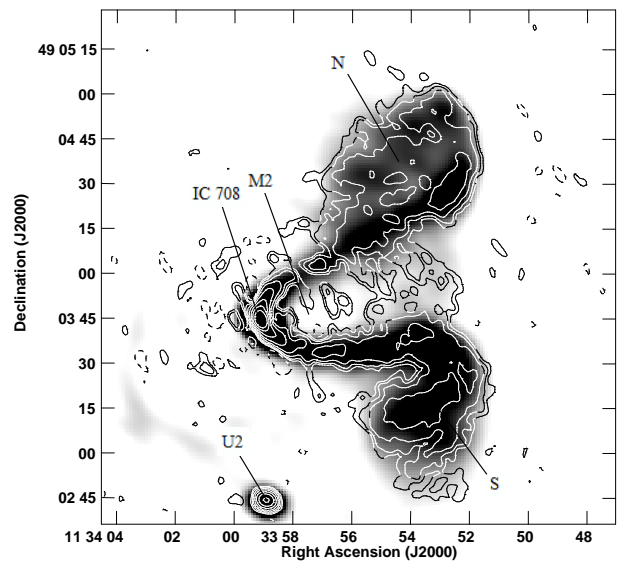


Figure 5. 1300 MHz high resolution map superimposed on the 610 MHz grey scale map of IC708. The contour levels are $0.06 \times (-4, 4, 8, 16, 32, 64, 128, 256, 512)$ mJy beam $^{-1}$.

(i.e., optical galaxies, see Fig. 4) on the tail along its long stretch.

Influence of the ICM seems to result in very different radio morphologies for the two neighbouring cluster members IC 708 and IC 711. Our high resolution 610 MHz map shows that the radio tail along its stretch is initially straight for two-thirds of its length, then there is a sharp (almost a 90°) bend, and then further along there is another similar sharp bend pointing away from the cluster center, which does not seem to be consistent with a simple circular motion around the cluster center.

According to Vallée (1988), the radio-tail hypothesis of Miley et al. (1972) can explain the shape of the head-tail galaxy IC 711 due to it ploughing through the dense intra-cluster gas as it moves in a simple circular orbit around the Abell 1314 centre where IC 712 is located (Fig. 1). The low-resolution maps used by Vallée (1988) did not separate out the independent sources U3 and U4 from the diffuse tail of IC 711 (Fig. 1) and that made it look like somewhat circular morphology. Vallée’s (1988) numerical simulations conform to that picture, where one of the main ingredient in their numerical simulation was the orbital motion of the galaxy around the cluster center. But now with better angular resolutions we have not only resolved the two sources U3 and U4 as not parts of the long tail of IC 711, but also the long straight tail makes it unambiguously clear that it is not affected by any gravitational force of the center galaxy IC 712. Moreover the extreme sharpness of tail bends after ‘D’ and ‘E’ also makes it clear that these bends are not result of any gravitational effect of any individual galaxy or even that of the overall gravitational potential of the cluster members. Nor could one think that the galaxy IC 711 could have moved in past along a path F-E-D-C (Fig. 1), as no gravitational influence on the galaxy could have made it take a path with such sharp bends. It looks like that the sharp bends have been caused by some sort of ‘walls’ or rather dense medium near ‘D’ and ‘E’ points (Burns

Table 2. Minimum energy estimates from flux densities, spectral indices and angular sizes

Components	240 MHz	610 MHz	1300 MHz	α_{240}^{610}	α_{610}^{1300}	ψ_x	ψ_y	U_{\min}	B_{eq}	τ_{rad}
	mJy	mJy	mJy			"	"	10^{-13} erg cm $^{-3}$	μG	10^8 yr
(1)	(2)	(3)	(4)	(5)	(6)	(7)	(8)	(9)	(10)	(11)
IC 711A	41 \pm 4	30 \pm 3	22 \pm 2	0.35	0.4	-	-	-	-	-
IC 711 B to C	585 \pm 25	335 \pm 16	117 \pm 6	0.6	1.4	167	111	1.3	1.2	1.5
IC 711 C to D	573 \pm 23	236 \pm 13	27 \pm 3	1.0	3	445	56	1.4	1.2	1.5
IC 711 D to E	176 \pm 9	46 \pm 5	1 \pm 0.5	1.5	5	222	28	2.4	1.6	2.5
IC 711 E to F	143 \pm 8	18 \pm 2	< 0.5	2.2	> 5	167	28	2.6	1.7	2.5
IC 708 N	636 \pm 30	372 \pm 20	239 \pm 15	0.6	0.6	68	47	7.7	2.9	0.5
IC 708 S	577 \pm 28	383 \pm 18	228 \pm 14	0.45	0.7	66	47	7.4	2.8	0.5
IC 708	2072 \pm 60	1363 \pm 42	791 \pm 24	0.45	0.75	-	-	-	-	-
IC 712	69 \pm 4	46 \pm 3	24 \pm 2	0.9	0.9	-	-	-	-	-
U1	50 \pm 3	41 \pm 2	17 \pm 1	0.2	1.2	-	-	-	-	-
U2	103 \pm 5	58 \pm 3	34 \pm 2	0.6	0.7	-	-	-	-	-
U3	37 \pm 3	18 \pm 2	6 \pm 1	0.8	1.6	-	-	-	-	-
U4	31 \pm 3	25 \pm 2	14 \pm 2	0.2	0.8	-	-	-	-	-

Column 1: Radio source component; columns 2-4: the flux density of the source component at the frequency of observations in mJy; columns 5-6: Spectral index derived from the flux densities in columns 2-4; columns 7-8: angular size of the component along two perpendicular axes; columns 9: minimum energy value; column 10: Equipartition magnetic field value; column 11: radiative life time of the source component.

1986). The presence of radio sources U3 close to ‘D’ as well as U4 at ‘E’ could have been those ‘walls’. For one thing there appears to be no splatter where the jet or tail encounters ‘wall’. Further, there are no optical counterparts of either of these sources to confirm them as cluster members and either or both of them could be foreground or background sources, though their presence close to the locations ‘D’ as well as ‘E’ are suggestive of some connection with the sharp bending. Another chance coincidence seems to be that four optically unidentified, prominent radio sources U1, U2, U3, U4 (Fig. 1) seem to lie within a few degrees in a straight line over a separation of 10 arcmin. This is a chance coincidence is corroborated by the fact that while U1 has a double radio structure quite close to this straight line joining these four sources, U3 shows a double radio structure almost perpendicular to this straight line.

The spectral index of the head (A) of IC 711 is flat ($\alpha \approx 0.4$; defined as $S \propto \nu^{-\alpha}$) between 240 and 1300 MHz (Table 2), while the spectral index of the tail steadily steepens as we move away from the head (Table 2). The closer parts of the tail (B to C and C to D; Fig. 1) are having still a normal spectra between 240 and 610 MHz, but the spectra of these parts of the tail is quite steep between 610 and 1300 MHz. But the remote parts of the tail (D to E and E to F) is rather steep between 240 and 610 MHz itself, and at frequencies higher than 610 MHz it is extremely steep ($\alpha \geq 5$). The closer parts of the tail may have break frequency not very far from 610 MHz, but the remote parts of the tail may have a break frequency more closer or even lower than 240 MHz. But since we have the detailed flux density measurements of the different parts of the tail at only these three frequencies, we take 610 MHz as the break frequency for our calculations as we find the spectra differ at the lower and higher frequencies.

The luminosity of IC 711 at 610 MHz is 1.8×10^{24} W Hz $^{-1}$ while that of IC 708 is 3.6×10^{24} W Hz $^{-1}$. Thus both radio galaxies fall very well within the FRI luminosity range. In this case we have both a NAT as well as a WAT in the same cluster quite close to each other and on the same side of the cluster centre.

The minimum energy density for a synchrotron radio

source component having a spectral break is given by

$$U_{\min} = 4.5 \times 10^{-10} \left[\frac{(1+z)^{3.5} S_0 \nu_0^{0.5}}{\psi_x \psi_y s} \left\{ \frac{(\nu_1/\nu_0)^{-\alpha_1+0.5}-1}{\alpha_1-0.5} - \frac{(\nu_2/\nu_0)^{-\alpha_2+0.5}-1}{\alpha_2-0.5} \right\} \right]^{4/7} \text{ erg cm}^{-3} \quad (1)$$

(see Appendix A). Here z is the redshift, S_0 (Jy) is the flux density at the break frequency ν_0 (GHz), α_1 and α_2 are the spectral indices before and after the break, with ν_1 and ν_2 (GHz) as the lower and upper cut off frequencies presumably for the observed radio spectrum, ψ_x and ψ_y (arcsec) represent the size of the source component along its major and minor radio axes, and s is the path length through the component along the line of sight in kpc. In the case of IC 711, with its long head-tail radio morphology, we take it to be a bent cylinder and take its depth to be equal to its minor radio axis and thus s is calculated from ψ_y , the width of the tail. At a redshift of 0.034, for $H_0 = 70$ km s $^{-1}$ Mpc $^{-1}$ it scales to 0.67 kpc per arcsec. We have assumed an equal energy distribution between the electrons and the heavy particles, taken the volume filling factor to be unity and also assumed the pitch angle to be 90°. Apart from other things these are consistent with our objective of finding at least a minimum value estimate of the energy density in the radio source component.

The equipartition magnetic field B_{eq} is calculated from Equation (A15)

$$B_{\text{eq}} \approx B_{\min} = 3.3 U_{\min}^{0.5} G. \quad (2)$$

The estimates of the minimum energy densities and equipartition magnetic fields for different parts of the tail are given in Table 2. Here we have integrated the radio emission from 100 MHz to 10 GHz. It should be noted that the upper cut-off frequency value is less critical for the minimum energy estimates. Surprisingly minimum energy estimates appear a bit larger in the remote parts of the tail, i.e., tail parts lying between D and E or between E and F (Fig. 1). This is because the spectrum in each of these cases is already quite steep between 240 and 610 MHz and most likely the break frequency is much lower than our assumed 610 MHz. But we do not have any measurements of the flux densities of these tail

parts at still lower frequencies. The rather steep spectral index values between 240 and 610 MHz results in unusually larger number of electrons at lower cut-off frequency limit and thus much larger U_{\min} estimates. On the other hand for IC 708 N and S components or even of the whole radio source the spectrum is not steep (Table 2). In fact from the 5 GHz map of Vallée & Wilson (1976) it seems the break frequency for IC 708 N and S components is $\gtrsim 5$ GHz. Our integrated 1300 MHz flux density measurements 791 ± 24 mJy of IC 708 are consistent with the measurements 835 ± 80 mJy at 1.4 GHz by Wilson & Vallée (1977). Also our 610 MHz flux density value (1363 ± 42 mJy) is equally consistent with the value 1432 ± 70 mJy at 610 MHz, as measured by Vallée & Wilson (1976).

Assuming that the spectral break lies around 610 MHz, the synchrotron life-times of radiating electrons are calculated from

$$\tau_{syn} \approx 1.06 \left(\frac{B_{\perp}}{\mu\text{G}} \right)^{-1.5} \left(\frac{\nu^*}{\text{GHz}} \right)^{-0.5} \text{ Gyr} \quad (3)$$

(see Appendix B). Since we are using the equipartition magnetic field determined from Equation (2), where pitch angle was assumed to be 90° , to be consistent we put $B = B_{\perp}$ here also. Synchrotron life-times turn out to be about $7 - 10 \times 10^8$ yr.

However, following van der Laan & Perola (1969), if we include the inverse-Compton losses from the Cosmic Microwave Background Radiation (CMBR) with energy density U_R or the equivalent magnetic field, $B_R = \sqrt{8\pi U_R}$ we can write the radiative life-times as

$$\begin{aligned} \tau_{rad} \approx 1.06 \left(\frac{B_{\perp}}{\mu\text{G}} \right)^{0.5} \left[\left(\frac{B_{\perp}}{\mu\text{G}} \right)^2 + \frac{2}{3} \left(\frac{B_R}{\mu\text{G}} \right)^2 \right]^{-1} \\ \times \left(\frac{\nu^*(1+z)}{\text{GHz}} \right)^{-0.5} \text{ Gyr.} \end{aligned} \quad (4)$$

With $U_R = 4.2 \times 10^{-13}(1+z)^4 = 4.8 \times 10^{-13}$ erg cm $^{-3}$ and the equivalent magnetic field, $B_R = 3.25(1+z)^2 = 3.5 \mu\text{G}$, the radiative life-times are about an order of magnitude lower $\sim 1.5 \times 10^8$ yr (Table 2). For estimating the radiative life times of the tail parts between D and E or between E and F, we have taken the break frequency to be 240 MHz, which we think is a more realistic value than 610 MHz. The projected distance of the tail end from the head is ~ 700 kpc, which would take $\gtrsim 5 \times 10^8$ yr for the galaxy IC 711 moving within the cluster with a velocity ~ 1200 km s $^{-1}$ (Coleman et al. 1976). The over all source must be in the sky plane, otherwise the ‘longest tail’ will be still longer. Coleman et al. (1976) have estimated that IC 711 radio tail may be making an angle of $\sim 20^\circ$ with respect to the sky plane and then its physical length will be about $1/\cos 20 \sim 10\%$ longer than that the projected length observed in the sky plane.

Now the radiative life-times of $\sim 10^8$ yr are inconsistent with the presumed absence of any re-acceleration occurrence in the tail parts as it is unlikely that energy could be continually supplied by the head (main galaxy) to its much lagging behind tail parts, especially through the two sharp bends. Here it should be noted that at about half a billion years further back, the CMBR energy density and the equivalent magnetic field would be

stronger which would make the inverse-Compton losses from the CMBR to be still higher and consequently the radiative life-times to be shorter about 10 percent than those in Table 2. As explained earlier, for calculating radiative life times for IC 708 N and S components in Table 2 we have used 5 GHz as the break frequency.

For both IC 711 and IC 708, twin jets start from the compact head almost in the same way (Figs. 2 and 5) and which conform to the basic model of jet-bending by Begelman et al. (1979), but in case of IC 711 they soon merge together to form a single tail while in case of IC 708 they stay separate in the WAT morphology and end up as individual lobes. It is still not clear what really decides the formation of these very distinct morphologies. IC 708 as compared to IC 711 is of course order of magnitude smaller in size (unless geometric projections play a major role). From Coleman et al. (1976), their parent optical galaxies do not seem to differ much in their speeds of motion within the cluster. It does not seem that the ICM density could have very large gradients to cause large difference at the positions of these two radio galaxies. This is because IC 711 at least samples a fairly large fraction of the cluster expanse and its tail does not seem to vary much in its width over its large extent. Their estimates of U_{\min} do differ by about a factor of three (Table 2).

In addition to IC 711 and IC 708, another cluster member, IC 712, the galaxy near the center of the cluster, has an unresolved radio source associated with it which has a normal radio spectrum. Further, there are four optically unidentified radio sources, U1, U2, U3 and U4 (Fig. 1), which do not seem associated with any of the cluster members and most likely are independent background radio sources. U1 possesses a clear double structure but surprisingly shows a flat spectrum between 240 and 610 MHz. U2, a normal spectrum radio source (Table 2), lies an arcmin south of IC 708 (Fig. 5) but is quite clearly not associated with it. U3 and U4 could of special interest as each of them lies very close to one of the two sharp bends seen in the radio tail of IC 711 (Fig. 1). However their optically unidentified nature as well as a clear double radio structure of U3 and the fact that U4 is an unresolved flat spectrum radio source, makes both of them unrelated to IC 711 (or even to the Abell cluster 1314 itself) and their closeness in sky positions to tail-bends of IC 711 are mere chance coincidences.

Radio tail of IC 711 not only seems to be straight most of its length (except for the two sharp bends mentioned earlier), it also seems to remain confined to quite a narrow width without any lateral free-expansion of the tail material, perhaps confined by the pressure of the ICM. The minimum energy of the tail may be used to estimate the pressure in the ICM, whose emissivity is otherwise not directly detectable, by assuming that the diffuse parts of the radio tail are in pressure equilibrium with it. The pressure of such a hot, diffuse, non-relativistic ICM could be thus estimated. Our estimate for the pressure in the tail part yields $P \sim 2 \times 10^{-13}$ dyne cm $^{-2}$ under the assumption of minimum energy in the radio tail and its pressure balance with the ICM in the cluster.

4. CONCLUSIONS

We presented low-frequency, GMRT observations at 240, 610 and 1300 MHz of IC 711, a long head-tail radio

galaxy, perhaps the longest known head-tail radio galaxy. Our high resolution 610 MHz map showed a long straight tail of angular extent ~ 10 arcmin, and later two sharp bends in the tail. The radio structure, especially the long straight tail, does not seem to be consistent with a simple circular motion around the cluster centre, as previously suggested in the literature. Each of the bends in the tail of IC 711 seems to occur very close to a prominent radio source, though it is not sure whether either of the bend is really related to the respective radio object. We are not even sure whether the radio sources close to the bends are cluster members, since no optical galaxy is found at either of them. Therefore either or both of these two radio sources could be background or even foreground

object, though the bending of the tail so close to them in sky is a very striking feature.

ACKNOWLEDGEMENTS

We thank the staff of the GMRT that made these observations possible. GMRT is run by the National Centre for Radio Astrophysics of the Tata Institute of Fundamental Research. This research has made use of the NASA/IPAC extragalactic database (NED) which is operated by the Jet Propulsion Laboratory, Caltech, under contract with the National Aeronautics and Space Administration.

APPENDIX

A. MINIMUM ENERGY CALCULATIONS IN THE CASE OF A SPECTRAL BREAK

We derive here an expression for minimum energy in a synchrotron source where a break is seen in the power-law spectrum of the observed flux-density. Such a break can occur in the synchrotron spectrum due to radiation losses in the case where, e.g., there is an isotropic distribution of electrons or if in the radiating region there is a continuous injection of fresh electrons with a power law energy distribution (Kardashev 1962; Pacholczyk 1970). We use cgs system of units throughout.

A relativistic electron of rest mass m_0 and energy E (corresponding to a Lorentz factor γ), gyrating in a uniform magnetic field B with a gyro frequency $\nu_g = \omega_g/2\pi = eB/(2\pi m_0 c \gamma)$, emits most of its radiation in a narrow frequency band around its characteristic synchrotron frequency (Rybicki & Lightman 1979)

$$\nu_c = \frac{3}{2} \nu_g \sin \theta \gamma^3 = \frac{3}{4\pi} \frac{e B_\perp}{m_0 c} \gamma^2 = c_1 B_\perp E^2. \quad (\text{A1})$$

where $c_1 = 3e/(4\pi m_0^3 c^5) = 6.26 \times 10^{18}$ (Pacholczyk 1970) and θ is the pitch angle. Accordingly, with the assumption that almost all the radiation from an electron is at a frequency $\nu \approx \nu_c$, we can write a one-to-one relation between the frequency at which synchrotron radiation is being emitted and the energy E of the electron emitting that radiation

$$E \approx \left(\frac{\nu}{c_1 B_\perp} \right)^{1/2}. \quad (\text{A2})$$

In radio sources, the observed flux density in the optically thin part of the spectrum usually follows a power law, i.e., $I_\nu \propto \nu^{-\alpha}$, between the lower and upper cut off frequencies ν_1 and ν_2 . In synchrotron theory this spectrum results from a power law energy distribution of radiating electrons $N(E) = N_0 E^{-\xi}$ within some range E_1 and E_2 , with $\xi = 2\alpha + 1$ and E_1, E_2 related to ν_1, ν_2 by Equation (A2). In the case of a spectral break at say, ν_0 , there may be spectral indices α_1 between ν_1 and ν_0 and α_2 between ν_0 and ν_2 , corresponding to energy indices ξ_1 between E_1 and E_0 and ξ_2 between E_0 and E_2 .

Now the energy distribution of radiating electrons cannot be written simply as $N(E) = N_0 E^{-\xi_1}$ between E_1 and E_0 and $N(E) = N_0 E^{-\xi_2}$ between E_0 and E_2 , as it will give $N(E_0) = N_0 E_0^{-\xi_1} = N_0 E_0^{-\xi_2}$ forcing $\xi_1 = \xi_2$. Instead we can write it as $N(E) = N_0 (E/E_0)^{-\xi_1}$ and $N(E) = N_0 (E/E_0)^{-\xi_2}$ for the two ranges with N_0 as the number density at E_0 .

A highly relativistic electron ($\gamma \gg 1$) radiates power at a rate (Melrose 1971; Jackson 1975; Longair 2011)

$$dE/dt = c_2 B_\perp^2 (1 - 1/\gamma^2) E^2 \approx c_2 B_\perp^2 E^2, \quad (\text{A3})$$

where $c_2 = 2e^4/(3m_0^4 c^7) = 2.37 \times 10^{-3}$ (Pacholczyk 1970).

Then luminosity L for such a synchrotron source is given by,

$$L = V \phi N_0 c_2 B_\perp^2 \left[\int_{E_1}^{E_0} (E/E_0)^{-\xi_1} E^2 dE + \int_{E_0}^{E_2} (E/E_0)^{-\xi_2} E^2 dE \right] \quad (\text{A4})$$

where V is the volume of the source and ϕ is the volume filling factor.

$$L = V \phi N_0 c_2 B_\perp^2 E_0^3 \left[\frac{(E_1/E_0)^{-\xi_1+3} - 1}{\xi_1 - 3} - \frac{(E_2/E_0)^{-\xi_2+3} - 1}{\xi_2 - 3} \right]. \quad (\text{A5})$$

Using Equation (A2), we can write

$$L = \frac{V \phi N_0 c_2 \nu_0^{1.5} B_\perp^{0.5}}{2c_1^{1.5}} \left[\frac{(\nu_1/\nu_0)^{-\alpha_1+1} - 1}{\alpha_1 - 1} - \frac{(\nu_2/\nu_0)^{-\alpha_2+1} - 1}{\alpha_2 - 1} \right] \quad (\text{A6})$$

The flux-density can also be written as $S_0(\nu/\nu_0)^{-\alpha_1}$ and $S_0(\nu/\nu_0)^{-\alpha_2}$ for the two ranges $\nu_1 - \nu_0$ and $\nu_0 - \nu_2$, with S_0 as the flux-density at ν_0 . Then the luminosity of such a source can be evaluated from the observed flux density at the spectral break as

$$L = 4\pi D_L^2 S_0 \left[\int_{\nu_1}^{\nu_0} (\nu/\nu_0)^{-\alpha_1} d\nu + \int_{\nu_0}^{\nu_2} (\nu/\nu_0)^{-\alpha_2} d\nu \right], \quad (\text{A7})$$

or

$$L = 4\pi D_L^2 S_0 \nu_0 \left[\frac{(\nu_1/\nu_0)^{-\alpha_1+1} - 1}{\alpha_1 - 1} - \frac{(\nu_2/\nu_0)^{-\alpha_2+1} - 1}{\alpha_2 - 1} \right] \quad (\text{A8})$$

From Equations (A6) and (A8) we can evaluate N_0 as

$$N_0 = \frac{8\pi c_1^{1.5} D_L^2 S_0}{c_2 V \phi B_{\perp}^{0.5} \nu_0^{0.5}} \quad (\text{A9})$$

Energy density of the relativistic electrons in a synchrotron radio source is given by

$$U_e = N_0 \left[\int_{E_1}^{E_0} (E/E_0)^{-\xi_1} E dE + \int_{E_0}^{E_2} (E/E_0)^{-\xi_2} E dE \right] \quad (\text{A10})$$

or

$$U_e = N_0 E_0^2 \left[\frac{(E_1/E_0)^{-\xi_1+2} - 1}{\xi_1 - 2} - \frac{(E_2/E_0)^{-\xi_2+2} - 1}{\xi_2 - 2} \right] \quad (\text{A11})$$

Using Equation(A2), energy density of the relativistic electrons in a synchrotron radio source is then given by

$$U_e = \frac{N_0 \nu_0}{2c_1 B_{\perp}} \left[\frac{(\nu_1/\nu_0)^{-\alpha_1+0.5} - 1}{\alpha_1 - 0.5} - \frac{(\nu_2/\nu_0)^{-\alpha_2+0.5} - 1}{\alpha_2 - 0.5} \right], \quad (\text{A12})$$

the expression to be evaluated in 'limit' if any of the α 's = 0.5.

Substituting N_0 from Equation (A9), we get

$$U_e = \frac{4\pi D_L^2 S_0 \nu_0^{0.5} c_1^{0.5}}{V \phi c_2 B_{\perp}^{1.5}} \left[\frac{(\nu_1/\nu_0)^{-\alpha_1+0.5} - 1}{\alpha_1 - 0.5} - \frac{(\nu_2/\nu_0)^{-\alpha_2+0.5} - 1}{\alpha_2 - 0.5} \right]. \quad (\text{A13})$$

The magnetic field energy density is $U_m = B^2/8\pi$. Therefore total energy density of the source is $U_t = (1+k)U_e + U_m = aB^{-1.5} + bB^2$, where k represents the factor for energy in heavier particles (baryons), which may range anything from 1 to 2000 or so. It should be noted that if the plasma comprises both electrons and positrons (a pair plasma), then $k=0$, as N_0 includes both electrons and positrons whose contributions are indistinguishable in incoherent synchrotron cases (Singal 2012). The expression for energy density is similar to as in the standard case of a single spectral index (Pacholczyk 1970; Moffet 1972), except that the co-efficient a is somewhat different.

After minimizing the total energy with B , we get

$$U_{\min} = 3.0 \times 10^{-10} \left[\frac{(1+k)(1+z)^{3.5} S_0 \nu_0^{0.5}}{\phi \psi_x \psi_y s \sin^{1.5} \theta} \left\{ \frac{(\nu_1/\nu_0)^{-\alpha_1+0.5} - 1}{\alpha_1 - 0.5} - \frac{(\nu_2/\nu_0)^{-\alpha_2+0.5} - 1}{\alpha_2 - 0.5} \right\} \right]^{4/7} \text{ erg cm}^{-3}. \quad (\text{A14})$$

Here z is the redshift, S_0 (Jy) is the flux density at the break frequency ν_0 (GHz), α_1 and α_2 are the spectral indices (defined as $S \propto \nu^{-\alpha}$) before and after the break, with ν_1 and ν_2 (GHz) as the lower and upper cut off frequencies presumably for the observed radio spectrum, ψ_x and ψ_y (arcsec) represent the size of the source component along its major and minor radio axes, and s is the path length through the component along the line of sight in kpc. It should be noted that the expression within curly brackets on the right hand side in Equation (A14) is independent of redshift if ν_1, ν_0, ν_2 are all in observer's frame, determined, for instance, from observations.

The magnetic field value corresponding to the minimum energy is given by

$$B_{\min} = \left[\frac{24\pi U_{\min}}{7} \right]^{0.5} = 3.3 U_{\min}^{0.5} G. \quad (\text{A15})$$

It should be noted that B_{\min} is not the minimum value of the magnetic field in the source under consideration. In fact it yields nearly the equipartition value of the magnetic field.

For a single spectral index case, where S_0 is the flux density at any frequency ν_0 with $\nu_1 < \nu_0 < \nu_2$, we put $\alpha_1 = \alpha_2 = \alpha$ in Equation (A14) to get,

$$U_{\min} = 3.0 \times 10^{-10} \left[\frac{(1+k)(1+z)^{3.5} S_0 \nu_0^{\alpha}}{\phi \psi_x \psi_y s \sin^{1.5} \theta} \left\{ \frac{\nu_1^{-\alpha+0.5} - \nu_2^{-\alpha+0.5}}{\alpha - 0.5} \right\} \right]^{4/7} \text{ erg cm}^{-3}. \quad (\text{A16})$$

If ν_1 and ν_2 represent the cut-off frequency values in the rest frame of the source (specified based on some other arguments), then the factor $(1+z)^{3.5}$ in Equation (A16) gets replaced with $(1+z)^{3+\alpha}$ to yield the same expression as available in the literature (Miley 1980; Singal et al. 2004).

B. THE PITCH ANGLE PARADOX AND RADIATIVE LIFE TIMES IN A SYNCHROTRON SOURCE

In synchrotron radiation there is a paradox whether or not the pitch angle of a radiating charge varies. The conventional wisdom is that the pitch angle does not change during the radiation process. Since the radiation is confined to a narrow cone of angle $1/\gamma$ around the instantaneous direction of motion of the charge, (Jackson 1975; Pacholczyk 1970; Rybicky & Lightman 1979), any radiation reaction on the charge will be in a direction just opposite to its instantaneous velocity vector. This means that the direction of motion of the charge will remain unaffected, implying no change in the pitch angle of the charge (Kardashev 1962; Pacholczyk 1970). The accordingly derived formulas for energy losses of synchrotron electrons in radio galaxies are the standard text-book material for the last 50 years. However, using the momentum transformation laws from special relativity, we shall show that the pitch angle of a radiating charge varies. While the velocity component parallel to the magnetic field remains unaffected, the perpendicular component does reduce in magnitude due to radiative losses, implying a change in the pitch angle.

With the pitch angle as a constant of motion, half life-times of radiating electrons have been calculated (Kardashev 1962; Pacholczyk 1970; Rybicki & Lightman 1989), using a radiation power loss formula

$$\frac{d\gamma}{dt} = -\eta \sin^2 \theta \gamma^2. \quad (\text{B1})$$

Here $\eta = 2e^4 B^2 / (3m_e^3 c^5) = 1.94 \times 10^{-9} B^2 \text{ s}^{-1}$. If γ_0 represents the initial energy at $t = 0$, then from Equation (B1) the energy of the radiating charge at $t = \tau$ becomes

$$\gamma = \frac{\gamma_0}{1 + \eta \sin^2 \theta \tau \gamma_0}. \quad (\text{B2})$$

It follows that energy of the electron reduces to half its value in time $\tau_{1/2} = 1/(\eta \sin^2 \theta \gamma_0)$ (Kardashev 1962; Kellermann 1964; van der Laan & Perola 1969; Pacholczyk 1970; Miley 1980).

However from Equation (B2) one can easily see that while it might be true for a highly relativistic charge ($\gamma \gg 1$), it cannot be a general result. This is because from Equation (B2) $\gamma \rightarrow 0$ when $\tau \rightarrow \infty$, while we know that $\gamma \geq 1$ always. Actually an approximation $\beta \approx 1$ has been used in Equation (B1); the exact equation for the energy loss rate (Melrose 1971; Jackson 1975; Longair 2011) is

$$\frac{d\gamma}{dt} = -\eta \sin^2 \theta \beta^2 \gamma^2 = -\eta \sin^2 \theta (\gamma^2 - 1). \quad (\text{B3})$$

Now, consider a charge particle in its gyrocenter (GC) frame \mathcal{K}' , where the charge has no component of velocity parallel to the magnetic field and has only a circular motion in a plane perpendicular to the magnetic field (with a pitch angle $\theta = \pi/2$). In this frame, due to radiative losses by the charge, there will be a decrease in the velocity which is solely in a plane perpendicular to the magnetic field, and the charge will never ever attain a velocity component parallel to the magnetic field because of radiation losses.

Now we look at this particle from the lab frame \mathcal{K} , in which the charge has (at least to begin with) a motion, β_{\parallel} along the magnetic field. Since in the inertial frame \mathcal{K}' , the charge never gets a velocity component parallel to the magnetic field and the two inertial frames (\mathcal{K} and \mathcal{K}') continue to move with reference to each other with a constant β_{\parallel} , the parallel component of velocity of the charge should remain unchanged even in \mathcal{K} . However, magnitude of the perpendicular component of velocity is continuously decreasing because of radiative losses, therefore the pitch angle of the charge, $\theta = \tan^{-1}(\beta_{\perp}/\beta_{\parallel})$, should decrease continuously with time and the velocity vector of the charge should increasingly align with the magnetic field vector. Thus we have a paradox here. While an argument based on the standard picture of Larmor's radiation losses had led us to the conclusion that the pitch angle of the charge is a constant, the later argument from relativistic transformation considerations showed that as the charge radiates its pitch angle could be progressively reducing with time.

In Equation (B3) $\sin \theta$ is a variable in the lab frame \mathcal{K} , but we can write this equation for the GC frame \mathcal{K}' , where pitch angle is always a constant ($\theta' = \pi/2$). Then we have

$$\frac{d\gamma'}{dt'} = -\eta \beta'^2 \gamma'^2 = -\eta (\gamma'^2 - 1). \quad (\text{B4})$$

Now Equation (B4) has a solution

$$\tanh^{-1} \frac{1}{\gamma'} = \eta t' + a. \quad (\text{B5})$$

Let γ'_0 be the initial energy at $t' = 0$ in frame \mathcal{K}' , then $1/\gamma'_0 = \tanh(a)$ and at time $t' = \tau'$ we have

$$\tanh^{-1} \frac{1}{\gamma'} = \tanh^{-1} \frac{1}{\gamma'_0} + \eta \tau'. \quad (\text{B6})$$

which complies with the expectations that as $\tau' \rightarrow \infty$, $\gamma' \rightarrow 1$.

A transformation between \mathcal{K}' and \mathcal{K} gives $\gamma'\gamma_{\parallel} = \gamma$ and $\gamma'\beta' = \gamma\beta_{\perp}$ or $\beta' = \gamma_{\parallel}\beta_{\perp}$ (Melrose 1971), where $1/\gamma_{\parallel} = \sqrt{1 - \beta_{\parallel}^2}$. Also we have $dt/dt' = \gamma_{\parallel}$ or $\tau = \tau'\gamma_{\parallel}$. For the transformation of acceleration we then get $\dot{\beta}' = \gamma_{\parallel}^2 \dot{\beta}_{\perp}$ with $\dot{\beta}_{\parallel} = \dot{\beta}'/\gamma_{\parallel}^3 = 0$.

Equation (B6) can be transformed in terms of quantities expresses in the lab frame \mathcal{K}

$$\tanh^{-1} \frac{\gamma_{\parallel}}{\gamma} = \tanh^{-1} \frac{\gamma_{\parallel}}{\gamma_o} + \frac{\eta\tau}{\gamma_{\parallel}}. \quad (\text{B7})$$

Thus we get γ as a function of time, starting from an initial γ_o .

Equation (B4) can be also written as

$$\gamma'^3 \dot{\beta}' \beta' = -\eta \beta'^2 \gamma'^2, \quad (\text{B8})$$

It should be noted that magnetic field does no work and any change in γ' is only due to the radiation losses and $\dot{\beta}'$ is in a direction opposite to β' in the GC frame.

We simplify Equation (B8) to write

$$\frac{\dot{\beta}'}{\beta'} = \frac{-\eta}{\gamma'}. \quad (\text{B9})$$

Then transforming to the lab frame \mathcal{K} we have

$$\frac{\dot{\beta}_{\perp}}{\beta_{\perp}} = \frac{-\eta}{\gamma}. \quad (\text{B10})$$

Both β and θ appearing in $\beta_{\perp} = \beta \sin \theta$ are functions of time. Also $\dot{\beta}_{\parallel} = d(\beta \cos \theta)/dt = 0$. Thence we get

$$\frac{d\theta}{dt} = \frac{-\eta \sin 2\theta}{2\gamma}, \quad (\text{B11})$$

which gives us the rate of change of pitch angle with time.

The expressions for the pitch angle changes and the radiation losses could be derived in an alternate way directly from the radiation reaction force (Singal 2016), where it is also shown that $1/\eta$ is the characteristic decay time of a synchrotron electron over which it not only turns from ultra relativistic into mildly relativistic one, but due to the change in the pitch angle during this time, its velocity vector also moves outside the angle $1/\gamma_o$ around the line of sight towards the observer.

However, on a much shorter time scale $\tau \sim 1/(\gamma_o \eta)$ where $\gamma_o \gg 1$ and for not too small a pitch angle, $\sin \theta_o \gg 1/\gamma_o$, implying $\gamma_{\parallel}/\gamma_o \ll 1$ (as $1/\gamma_{\parallel} = \sqrt{1 - \beta_o^2 \cos^2 \theta_o} \approx \sin \theta_o$), from Equation (B7) we could write

$$\frac{1}{\gamma} = \frac{1}{\gamma_o} + \frac{\eta\tau}{\gamma_{\parallel}^2}, \quad (\text{B12})$$

or

$$\gamma = \frac{\gamma_o}{1 + \eta\tau\gamma_o/\gamma_{\parallel}^2} = \frac{\gamma_o}{1 + \eta\tau\gamma_o \sin^2 \theta_o}. \quad (\text{B13})$$

Equation (B13) is the same relation as Equation (B2), but which now we know is valid only for $\gamma_o \gg 1$, $\tau \lesssim 1/(\gamma_o \eta)$ and for pitch angle not too small ($\sin \theta_o \gg 1/\gamma_o$).

From Equations (B12) and (B13) it is easily seen that irrespective of the initial energy γ_o of the radiating electron at time $t = 0$, at a later time $t = \tau$, its energy will have an upper limit $\gamma^* = 1/\eta\tau \sin^2 \theta_o$. This in turn tells us about the radiating life-times of the synchrotron electrons

$$\tau_{syn} \approx \frac{16}{B_{\perp}^2 \gamma^*} \text{ yr}. \quad (\text{B14})$$

From Equation (A1), a synchrotron electron with energy γ radiates around

$$\nu \approx 4.20 \times 10^6 B_{\perp} \gamma^2, \quad (\text{B15})$$

with an exponential drop in flux density above frequency ν . Therefore an upper limit γ^* implies an upper limit on frequency ν^* above which the flux density falls exponentially.

From a sharp steepening of the observed spectrum one gets the value of ν^* and then an estimate the age of the synchrotron source is obtained as

$$\frac{\tau_{syn}}{\text{yr}} = \frac{3.35 \times 10^4}{B_{\perp}^{1.5} \sqrt{\nu^*}} = 1.06 \times 10^9 \left(\frac{B_{\perp}}{\mu\text{G}} \right)^{-1.5} \left(\frac{\nu^*}{\text{GHz}} \right)^{-0.5}, \quad (\text{B16})$$

provided an estimate of magnetic field B is available, e.g., from the minimum energy estimates (Equation (A15)) which yields nearly an equipartition value of the magnetic field.

REFERENCES

- Begelman, M. C., Rees, M. J., & Blandford, R. D. 1979, *Nature*, 279, 770
 Burns, J. O. 1986, *Canadian Journal of Physics*, 64, 373
 Coleman, G. D., Hintzen P., Scott, J. S., & Tarengi, M. 1976, *Nature*, 262, 476
 Feretti, L. & Giovannini, G. 2008, *Lect. Notes Phys.*, 740, 143
 Jackson, J. D. 1975, *Classical electrodynamics*, 2nd ed., (New York: Wiley)
 Jägers, W. J. 1987 *A&ASS* 71, 603
 Kardashev, N. S. 1962, *Sov. Astr. - AJ*, 6, 317
 Kellermann, K. I. 1964, *ApJ*, 140, 969
 Longair, M. S. 2011, *High energy astrophysics*, (Cambridge: Cambridge Univ. Press)
 Melrose, D. B. 1971, *ApL*, 8, 35
 Miley G.K. 1980, *ARA&A*, 18, 165
 Miley G. K., Perola, G. C., van der Kruit, P. C., & van der Laan, H. 1972, *Nature*, 237, 269
 Moffet, A. T. 1975, in *Galaxies and the Universe (Stars and Stellar Systems, Volume IX)*, Ed. A. Sandage, M. Sandage, & J. Kristian, (Chicago: Univ. Chicago Press)
 O’Dea, C. P., & Owen, F. N. 1985, *AJ*, 90, 927
 Owen, F. N., & Ladlow, M. J. 1997, *ApJS*, 108, 41
 Pacholczyk, A. G. 1970, *Radio astrophysics*, (San Francisco: Freeman)
 Rybicki, G. B., & Lightman, A. P. 1979, *Radiative processes in astrophysics*, (New York: Wiley)
 Saripalli, L., Hunstead, R. W., Subrahmanyan, R., & Boyce E. 2005, *AJ*, 130, 896
 Singal, A. K. 2016, *MNRAS*, 458, 2303
 Singal, A. K., Konar, C., & Saikia, D. J. 2004, *MNRAS*, 347, L79
 Singal, A. K. 2012, *AJ*, 143, 131
 Vallée J. P. 1988, *Ap&SS*, 149, 225
 Vallée J. P., Bridle, A. H., & Wilson A. S., 1981, *ApJ* 250, 66
 Vallée J. P., & Strom R. G. 1988, *AJ*, 95, 1360
 Vallée J. P., & Wilson, A. S. 1976, *Nature*, 259, 451
 Vallée J. P., Wilson, A. S., & van der Laan, H. 1979 *A&A* 77, 183
 van der Laan & H. Perola, G. C. 1969, *A&A*, 3, 468
 Wilson, A. S., & Vallée J. P. 1977 *A&A* 58, 79